

Evaluation of Funnel Models on Calculation of Ion-Induced Collected Charge

Vitor A. P. Aguiar[®], Nilberto H. Medina[®], *Member, IEEE*, Nemitala Added[®], Saulo G. Alberton[®], Eduardo L. A. Macchione[®], Marcilei A. Guazzelli[®], *Member, IEEE*, Marco A. A. Melo, Juliano A. Oliveira, Renato C. Giacomini[®], *Member, IEEE*, Fernando R. Aguirre, Paula R. P. Allegro[®], Hellen C. S. Zaggato[®], and Isaac J. Sayeg

Abstract—Charge funneling is a widely used description of charge collection dynamics in semiconductor devices struck by ion irradiation, but it still relies on semiempirical parameters heavily dependent upon available data, which impacts its use for device or circuit-level simulations. The objective of this article is to analyze a comprehensive dataset from low-energy heavy-ion irradiations on a p-MOSFET, varying both the linear energy transfer (LET) and ion penetration depth within the device. A novel methodology is proposed to achieve this goal by analyzing devices without prior knowledge of their parameters, using data from light ion irradiations. Statistical analysis of the data and comparisons to simulated values showed that a LET-dependent funnel length is a more accurate description of the phenomenon than the conventional constant-length approach. A new, lower value for the funnel model's shielding parameter k was identified, and the method also allowed for determining the metal and passivation layer thicknesses of the device. These results strengthen the reliability of the funnel model, making it a more robust tool for simulation applications.

Index Terms—Charge collection, funneling, ion-induced charge, single-event transient.

I. INTRODUCTION

THE occurrence of transient signals induced by ionizing radiation has been studied for several years, but the description of the formation of these transient signals usually relies on TCAD simulations or semiempirical models [1], [2], [3], [4]. Despite their wide applicability, TCAD

Received 10 October 2024; revised 7 November 2024; accepted 11 November 2024. Date of publication 22 November 2024; date of current version 31 December 2024. This work was supported in part by Brazilian Agencies Comissão Nacional de Energia Nuclear (CNEN) and Conselho Nacional de Desenvolvimento Científico e Tecnológico (CNPq) under Grant Universal 404054/2023-4 and Grant INCT-FNA 464898/2014-5 and in part by Fundação de Amparo à Pesquisa do Estado de São Paulo (FAPESP) under Grant 2023/16053-8. The review of this article was arranged by Editor K. Stefanov. (Corresponding author: Vitor A. P. Aguiar.)

Vitor A. P. Aguiar, Nilberto H. Medina, Nemitala Added, Saulo G. Alberton, Eduardo L. A. Macchione, Fernando R. Aguirre, Paula R. P. Allegro, and Hellen C. S. Zaggato are with the Institute of Physics, University of Sao Paulo (USP), São Paulo 05508-090, Brazil (e-mail: vitor.angelo.aguiar@usp.br).

Marcilei A. Guazzelli is with the Department of Physics, Centro Universitário da FEI, São Bernardo do Campo 09850-901, Brazil.

Marco A. A. Melo, Juliano A. Oliveira, and Renato C. Giacomini are with the Department of Electrical Engineering, Centro Universitario da FEI, Sao Bernardo do Campo 09850-901, Brazil.

Isaac J. Sayeg is with the Institute of Geosciences, University of Sao Paulo (USP), Sao Paulo 05508-090, Brazil.

Digital Object Identifier 10.1109/TED.2024.3497927

simulations are time-consuming, require the knowledge of several characteristics of the device under study, and are strongly dependent on the physical models and approximations used, while the semiempirical models can straightforwardly provide meaningful information, even for circuit-level simulations [5]. Among such models, two descriptions of the charge-collection length (CCL), i.e., the depth within the device where the radiation-induced charge pairs are effectively collected, are common: the constant value and the funnel model.

The funnel model was first introduced in 1980 decade [2], [6], [7] and is based on the assumption that, under high carrier injection conditions, as observed in heavy-ion irradiations, and with impinging ion crossing the depletion region, the high concentration of charge carriers along the ionization tracks creates a temporary condition called "electron-hole plasma," a region of high conductivity that allows every charge carrier within this region to be transported to the depletion region and, thus, be collected. This model is, perhaps, the most used for explaining the charge collection induced by ions in semiconductor devices, and its introduction in simulations may be needed to match experimental data or perform circuit-level simulations [5], [8], [9], [10], [11], but it is not free of criticism, as in [12], [13], [14], and [15]. The proper description of ion-induced charge collection dynamics plays a significant role in understanding single-event transients also in new materials and technologies [16], [17], [18].

Despite the relative success of some semiempirical models, they rarely take into account the linear energy transfer (LET) variations as the incoming ion loses energy, because they are usually based on data obtained with high-energy ions [8], even though Monte Carlo simulations have shown its importance [19]. It is especially mandatory to consider this LET variation for low-energy heavy ions, as both the LET profile changes inside the silicon active layer and the energy loss in metal and passivation layers also contribute to rather different LET values in different parts of a device. However, careful consideration of energy losses in each layer of different materials that make up the device can provide insight into the charge collection processes and even a description of the device's characteristics. This becomes a highly relevant factor, particularly in the case of commercial off-the-shelf (COTS) devices, as such information is generally not readily available.

This work presents an investigation of the funnel model for charge collection in a p-MOSFET, using low-energy heavy ions as a radiation source. It provides a new methodology to describe the charge collection length (CCL) in the funnel model without prior knowledge of the device's parameters, using only the heavy-ion irradiation data. Besides the deeper understanding of funnel model limitations, the method also has led to a determination of the thicknesses of passivation and metal layers and can be useful for a better understanding of single-event phenomena.

II. CHARGE COLLECTION AND FUNNEL MODELING

In drift/funnel processes, the charge collection in semiconductor devices is defined as follows [7]:

$$Q_c = \frac{q}{w} \int_{x=0}^{L_{\text{eff}}} \frac{dE(x)}{dx} dx = q \int_{x=0}^{L_{\text{eff}}} \overline{N_0}(x) dx \tag{1}$$

where q is the elementary charge, w is the electron-hole pair creation energy, $L_{\rm eff}$ is the effective length of charge collection path, (dE(x)/dx) is the stopping power of incoming ion, and $\overline{N_0}$ is the mean density of electron-hole pairs along the track [6], [19], [20]. While collected charge depends on the funnel length, there is no analytical expression [20] for it, although there are also some semiempirical models, such as the one by Hu [3], [20], that express the funnel length as a function of the device parameters and independent of the incoming ion

$$L_f = \left(1 + \frac{\mu_n}{\mu_D}\right) \frac{W_D}{\cos\theta} \tag{2}$$

in which μ_n and μ_p are, respectively, electron and hole mobilities, W_D the depletion region width, and θ the incoming particle incidence angle. A more complex model by McLean and Oldham [6], [7], [20] states that funnel length [see (3)] depends on the duration of the electron-hole plasma τ_C [see (4)], on electron mobility μ_n , on the applied voltage V_0 , carrier density at track's beginning N_0 , and a factor named k, which was fit by the authors from experimental data to represent the shielding of electric field due to the high concentration of electron-hole pairs, especially important when analyzing data obtained with low-range ions (<14 μ m) [7]

$$L_f = \sqrt{\mu_n V_0 e^{-kN_0} \tau_C}.$$
(3)

The time constant, τ_C , also depends on N_0 , on the doping concentration N_A , the hole mean velocity v_P , and the ambipolar diffusion constant D. Proposed values for D, k, and v_P , for silicon, are as follows: 25 cm²/s, 1.3×10^{-10} cm/pair, and $(\mu_n V_0/W_D)$, respectively [7]. A detailed description of the model assumptions is out of the scope of this article, and the reader should refer to the original works

$$\tau_c = \left(\frac{3N_0}{8\pi N_A v_P \sqrt{D}}\right)^{2/3}.\tag{4}$$

TABLE I
IRRADIATION CONDITIONS: ION BEAMS, ENERGIES, EFFECTIVE
ENERGIES AT THE DEVICE'S SURFACE, RANGE,
AND SURFACE LET FOR SILICON

Ion	$Energy_A$	$\mathrm{Energy}_{\mathrm{eff}}$	Range	LET_{surf}
Beam	(MeV)	(MeV)	(μm)	$(\text{MeV.cm}^2/\text{mg})$
$^{12}\mathrm{C}$	35.0	33.9	38.2	2.9
	54.5	53.7	72.4	2.2
^{16}O	35.0	33.1	22.6	5.4
	42.0	40.2	28.5	5.0
	62.5	60.8	48.2	4.1
$^{19}\mathrm{F}$	42.0	39.7	23.2	6.5
	70.0	68.2	44.5	5.4
$^{28}\mathrm{Si}$	42.0	37.4	13.0	14.0
	60.0	55.5	18.8	12.8
	78.0	72.2	19.7	16.6
$^{35}\mathrm{Cl}$	42.0	36.3	10.8	18.1
	56.0	50.1	14.2	17.6
	78.0	72.2	19.7	16.6
$^{48}\mathrm{Ti}$	56.0	48.4	12.5	23.0
	78.0	70.0	15.5	23.8
$^{63}\mathrm{Cu}$	42.0	33.6	8.0	27.3
	49.0	40.2	9.0	28.6
	63.0	53.4	10.9	30.4
	78.0	67.8	12.9	31.4
	93.0	83.0	15.0	31.9
	110.0	98.4	17.0	32.0
$^{107}\mathrm{Ag}$	60.0	48.8	9.0	36.2
	110.0	95.6	13.8	46.0

III. TEST METHODOLOGY

The chosen MOSFET for analysis was a p-type 3N163 from Linear Integrated Systems [21], a device that has been investigated as a dosimeter [22], due to its response to TID effects, and SET signals on it were used for training neural networks for signal/noise classification [23].

The device under test (DUT) was decapsulated and positioned in a sample holder inside the high-vacuum chamber for frontside irradiation and biased with $V_{\rm DS} = -0.1~\rm V$ and $V_G = -4.5~\rm V$ for linear response. The drain contact was connected to the 50- Ω input of a digital oscilloscope (Rohde and Schwarz RTE 1104, 5 GSa/s, 1 GHz) to record transient pulse waveforms. The experiment was carried out in the SAFIIRA beamline [24] for uniform heavy-ion irradiation with a broad range of ion energies and species. SAFIIRA uses a combination of defocusing and multiple scattering to reduce beam intensity and increase uniformity, at the expense of having an effective energy of particles reaching the device lower than at the 8-MV tandem accelerator's exit.

To obtain a wide range of surface LET values (from about 2 MeV/mg/cm² up to approximately 45 MeV/mg/cm² on silicon) and different energy deposition profiles in the first tens of micrometers within the DUT, several ion beams and energies were used. Particle flux was kept lower than 3×10^5 part/s/cm², and whenever possible, statistical uncertainties were kept below 5%. In Table I, ion beam species, energies at accelerator exit, effective beam energy after multiple scattering, range, and surface LET in silicon are shown.

For all test conditions, 10^3 – 10^4 events were recorded. Low-LET ions led to fewer valid events, as a result of more frequent noise triggering.

To properly account for the energy loss of the ions in passivation/metal layers, thus before entering the sensitive

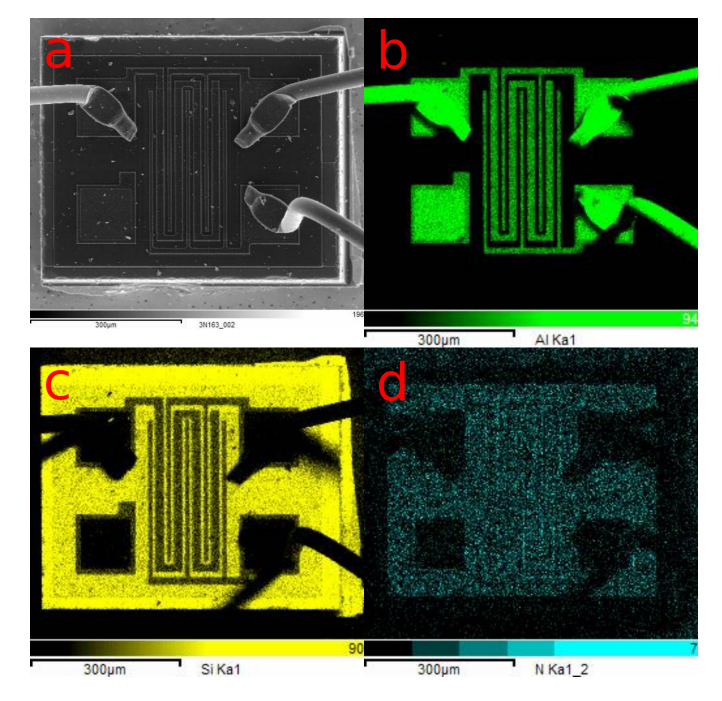


Fig. 1. Electron micrography and elemental mapping of p-MOSFET 3N163, at 20-kV acceleration voltage. (a) Secondary electron image. (b) Spatial distribution of aluminum. (c) Spatial distribution of silicon. (d) Spatial distribution of nitrogen.

volume, chemical composition information was obtained using scanning electron microscopy with energy-dispersive microanalysis (LEO 440i with Oxford EDS). Elemental mapping for Si, Al, and N is shown in Fig. 1, where it is seen that the drain, gate, and source metal contacts are made of aluminum, and there is a uniform nitrogen and silicon distribution, suggesting a passivation layer of silicon nitride (Si₃N₄). Quantitative chemical analysis for several acceleration voltages, thus changing the electron interaction depth, was performed to estimate the thickness of this layer. Measured stoichiometries were compatible with Si₃N₄ in a region of about 0.5–1.0- μ m thick. Oxygen content was below 5%.

IV. CHARGE SPECTROSCOPY ANALYSIS

After data filtering for noise rejection, each valid signal acquired was fit by a curve defined as the sum of three Gaussian functions for better reproduction of the signal shape. From each fit, signal amplitude, width, and area above baseline (charge) were obtained, and these parameters were organized in uni- and bi-dimensional histograms. Pulsewidth was taken as the standard deviation of the curve fit to the signal. Typical signals for ¹⁶O at 42 MeV and ⁶³Cu at 110 MeV ion beams are shown in Fig. 2, as well as a peak observed for ¹⁶O at 42 MeV along with baseline and signal fits and indication of the parameters analyzed.

For heavier ions, total charge and amplitude histograms were verified to be bimodal with a long tail of smaller values of charge collection. As can be seen in representative charge collection distributions in Fig. 3, the separation between the two peaks increases with Z at similar energies. Given that collected charge is proportional to deposited energy in the charge collection region, it suggests that not all incoming

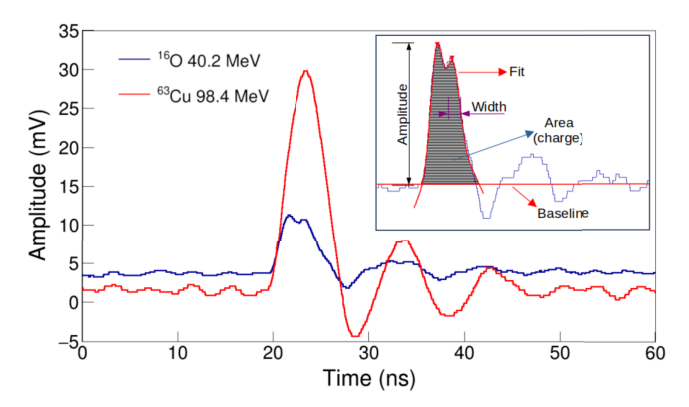


Fig. 2. Charge collection signals and fitted curves for ¹⁶O 42-MeV and ⁶³Cu 110-MeV initial energy. Effective energies are listed in Table I and presented in the legend. Inset: scheme of peak fitting and parameter extraction.

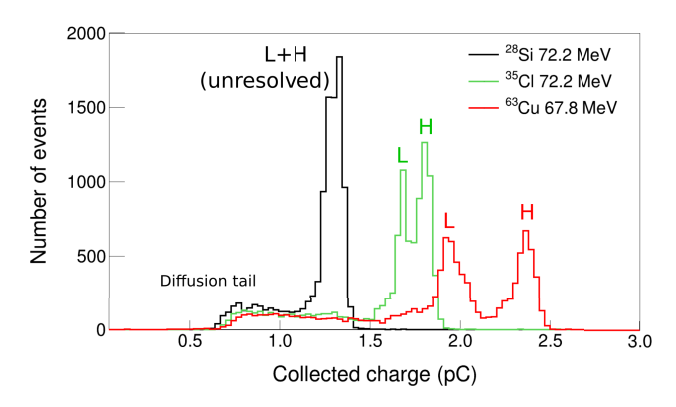


Fig. 3. Collected charge distributions for 28 Si, 35 Cl, and 63 Cu ion beams with 78-MeV initial energy. Effective energies are listed in Table I and presented in the legend. The peaks in the charge distribution indicated by H are relative to ions reaching the sensitive layer with higher energy, thus passing just through the Si_3N_4 layer. The peaks indicated by L are relative to ions reaching the sensitive layer with lower energy, thus passing through both Si_3N_4 and aluminum layers.

energy is converted into collected charge, due to energy losses in passivation/metal layers and possible variations in CCL. For light ions, charge and amplitude histograms are monomodal. Bidimensional histograms show a linear relationship between pulse amplitude and collected charge, as shown in Fig. 4, and also an almost constant pulsewidth, as shown in Fig. 5. Nevertheless, some data points do not follow this linear relationship in Fig. 4, corresponding to the events of larger pulse widths and lower and disperse charge values (bottom part of Fig. 5), also shown in the left part of each histogram in Fig. 3.

These results suggest that the charge collection in the p-MOSFET studied occurs by two processes with different collection times. The dominant and faster collection process is by drift/funneling, whereas the minority and slower process is by diffusion. As the collected charge is a measure of deposited energy in the sensitive region, the bimodal distribution also indicates an energy loss of some particles before entering the sensitive volume. For light ions, this energy change is negligible, but for heavier ions, this energy change needs to be accounted for. Also, considering an energy-charge conversion

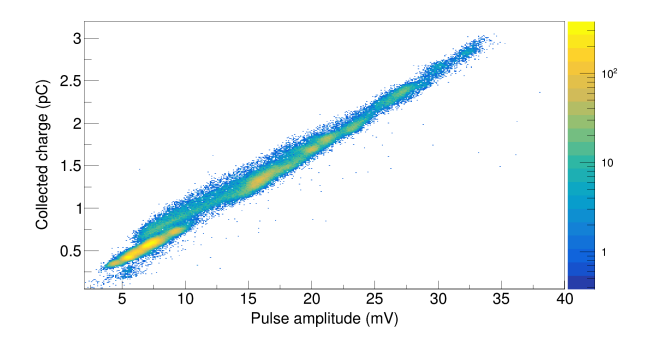


Fig. 4. Bidimensional distribution of charge x amplitude for all acquired signals.

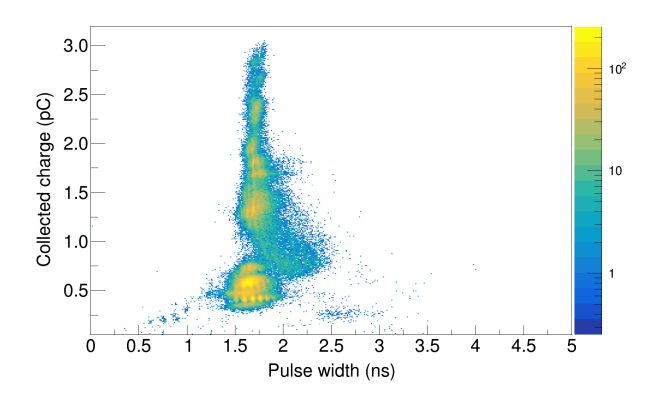


Fig. 5. Bidimensional distributions of charge x width for all acquired signals.

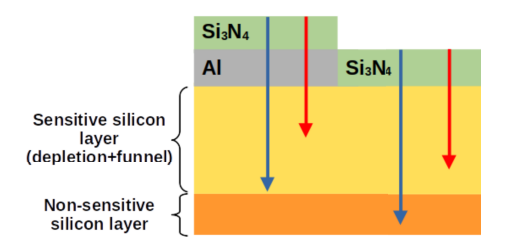


Fig. 6. Schematics of range and energy deposition along the track of incoming ions. Blue arrows represent long-range ions, and red arrows represent short-range ions. Sensitive layer thickness may be ion-dependent, if variable funnel model is considered.

factor of 22.6 MeV/pC [25], it is observed that not all of the ion's energy is collected, indicating a maximum sensitive depth in addition to energy losses before entering the sensitive region, as pictured in Fig. 6.

V. ENERGY DEPOSITION, LAYER THICKNESSES, AND CHARGE COLLECTION SIMULATIONS

Information from charge collection histograms and elemental mapping indicates that the bimodal distribution in the charge collection histograms can be explained by the energy difference of heavy ions that passed through the $\mathrm{Si}_3\mathrm{N}_4+\mathrm{Al}$ layers and only the $\mathrm{Si}_3\mathrm{N}_4$ layer. As heavier ions present higher stopping power values, the charge (energy) difference between the two peaks must increase with Z, therefore allowing the determination of the thickness of the aluminum layer. Considering the 22.6-MeV/pC charge-energy conversion factor in silicon material, the charge separation was converted into

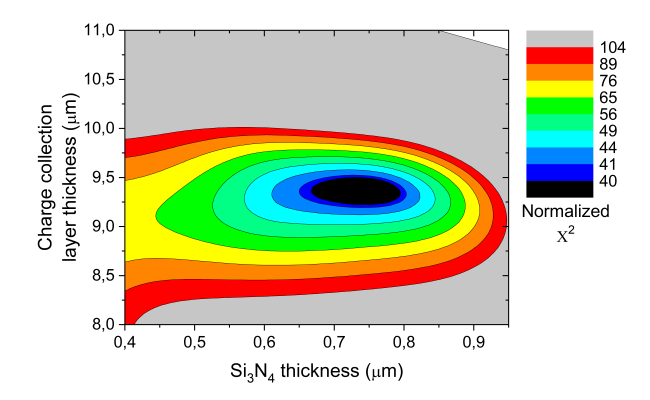


Fig. 7. Normalized χ^2 distribution as a function of Si₃N₄ and active layer thickness. Simulation steps were 0.05 μ m for Si₃N₄ and 0.2 μ m for active layer. Curves were smoothed by interpolation.

energy separation. Energy uncertainties were estimated by the standard deviation of individual peaks (split through a 2-D histogram cut) and the uncertainty arising from individual signal fitting (approx. 200 keV). SRIM software [26] was used to simulate the energy difference between the entrance and exit of the Al layer, for each ion-energy combination for which the bimodal distribution was observed. The best value was obtained by minimization of reduced residual, defined as the difference between simulated and measured values, divided by the uncertainty, and considering short-range ions, which resulted in a value of 1.28(2)- μ m aluminum thickness. The variation of the ion stopping power as a result of energy loss in the Si₃N₄ layer is negligible, given the uncertainties involved [26].

To obtain the CCL, it is necessary to account for every energy loss before the particle enters the sensitive region, including the energy loss in the Si_3N_4 layer, whose thickness was only estimated. The measured energy deposit along the charge collecting region was then compared with simulated values with SRIM, varying both Si_3N_4 and active silicon thickness. Two approaches for the active silicon thickness were used: constant value CCL for all ions and variable CCL based on the model by McLean and Oldham.

For a constant CCL, the values were changed with a fixed step in the simulations, and a chi-squared (χ^2) map was built (Fig. 7), from which one can see the independence of the variables. All sources of statistical errors were considered, but still, the χ^2 value was very high, indicating that the model is not a complete and statistically robust description of the phenomenon, but an analysis of accuracy can still be done. The χ^2 values in Fig. 7 were normalized by the number of degrees of freedom to reproduce only the data's accuracy, and the values obtained were $0.73(6) \mu m$ for Si_3N_4 thickness and 9.4(2) μm for the constant CCL model. For the minimum χ^2 condition, Fig. 8 presents the residual values as a function of the ion's range (in silicon, for simplicity), where it is seen that for short-range ions, residuals are not evenly dispersed around zero, therefore tendentious, indicating a possible dependence of charge collection thickness with ion energy and species.

The variable length funnel model, on the other hand, describes the CCL as a function of incoming ion and

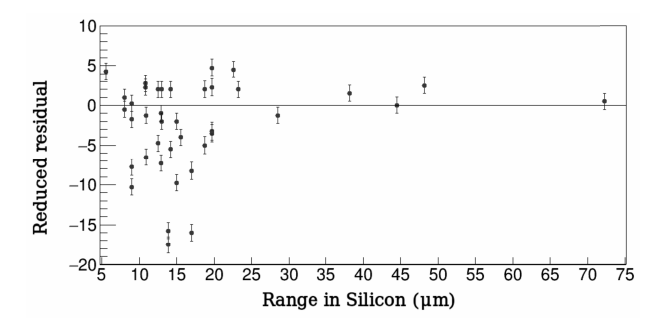


Fig. 8. Reduced residues for charge collected on the minimum χ^2 condition, as a function of the ion's range in silicon.

parameters of the device, such as doping level, depletion thickness, and so on, that were not available for the device in this study, which led to the development of a new methodology of analysis.

Combining (1) and (3) and considering that the mean density of electron-hole pairs along the ion track is the same as in its beginning, which especially holds for light ions, whose LET is almost constant up to tens of micrometers range, it is possible to write collected charge as a linear relationship with the device characteristics, represented by ψ

$$Q = q \overline{N_0} L_f$$

$$= q N_0 \sqrt{\mu_n V_0 e^{-kN_0}} \left(\frac{3N_0}{8\pi N_A v_P \sqrt{D}} \right)^{1/3}$$

$$\Longrightarrow q N_0^{4/3} \sqrt{e^{-kN_0}} \psi = \xi \psi$$
(5)

where ξ depends only on the ion and energy and $\psi = (3W_D/(8\pi N_A(\mu_n V_0 D)^{1/2}))^{1/3}$ is a constant that absorbs all device parameters. Fig. 9 illustrates the fit result of (5) for low-LET ions and its extrapolation for higher LET values. The points relative to heavier ions were taken, considering the charge distribution relative to ions that do not interact with aluminum (as the peaks marked with H in Fig. 3). The value for ψ obtained from curve fit was $6.78(88) \times 10^{-7}$ cm^{4/3}. This relationship allows the calculation of the funnel length and collected charge without any prior knowledge of the device parameters, such as doping level, voltage applied, and mobilities, and can be applied to different devices and materials, as long as data with light ions are available.

Using the variable length funnel model, the funnel length is given by (3), and the total collected charge in this path is increased by the amount of charge that can reach the funnel by diffusion, during its lifetime, as in (4). Using (5) to eliminate doping from the equation, for each value of shielding parameter k, the funnel length was calculated, the value obtained simulated with SRIM to obtain energy deposition and get collected charge. The comparison of SRIM simulations with measured data has shown that $k = 1.3 \times 10^{-10}$ cm/pair proposed by McLean et al. [7] was not adequate to reproduce the experiment results; instead, the best-fit condition was obtained with $k = 8.7(2) \times 10^{-11}$ cm/pair and Si₃N₄ thickness equal to 0.71(5) μ m, that also led to more evenly distributed reduced residuals (Fig. 10). Again, the χ^2 values were very high, so the values were normalized by the number of degrees of freedom

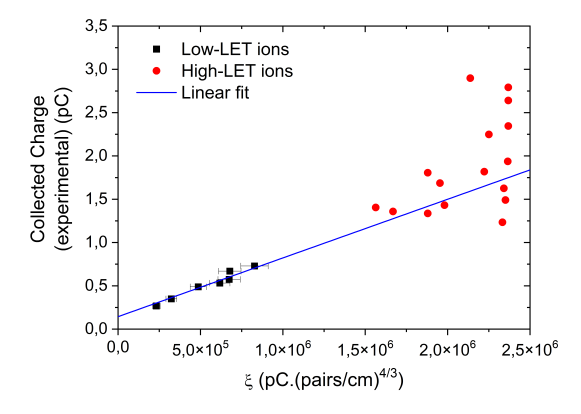


Fig. 9. Linear relationship between measured charge and the parameter ψ , dependent only on the device characteristics. The R^2 coefficient of the line is 0.96 for black data (light ions, long range) and 0.23 for red data (heavy ions, short range).

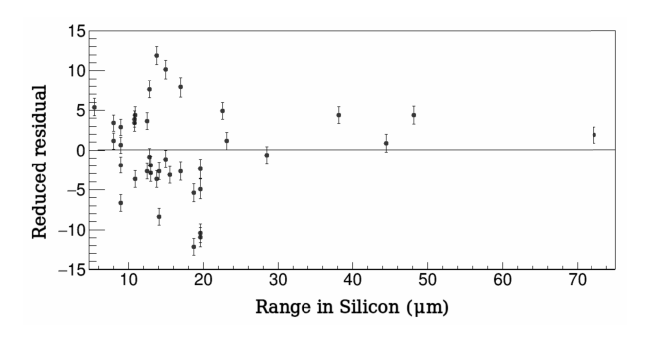


Fig. 10. Reduced residues for collected charge in the minimum χ^2 condition and variable length funnel with factor $k = 8.75 \times 10^{-11}$ cm/pair as a function of the ion's range in silicon.

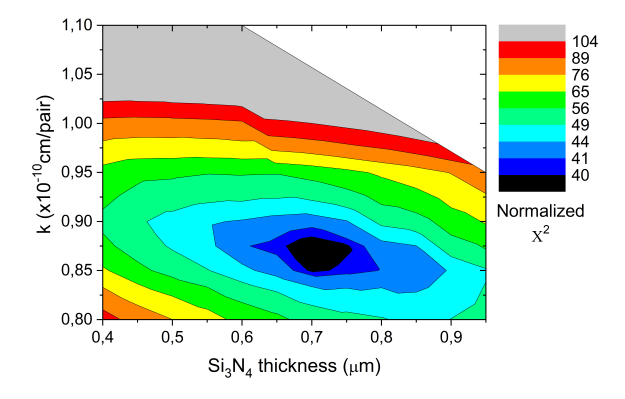


Fig. 11. Normalized χ^2 distribution as a function of Si₃N₄ thickness and k parameter value. Simulation steps were 0.05 μ m for Si₃N₄ and 0.25 \times 10⁻¹¹ cm/pair for k value.

to obtain uncertainties with \sim 68% confidence level. This k parameter should be different for different materials [7], but not for different doping levels or devices. The corresponding χ^2 map is shown in Fig. 11, where the inclination of the contour lines indicates that both parameters are correlated, as changes in Si₃N₄ thickness influence on the carrier density generation in the active region.

Finally, a simulation of the thickness of silicon in which the energy deposition provides the best agreement with experimental data, for each irradiation condition separately, in steps of 0.05 μ m, is shown in Fig. 12. The y-coordinates of the

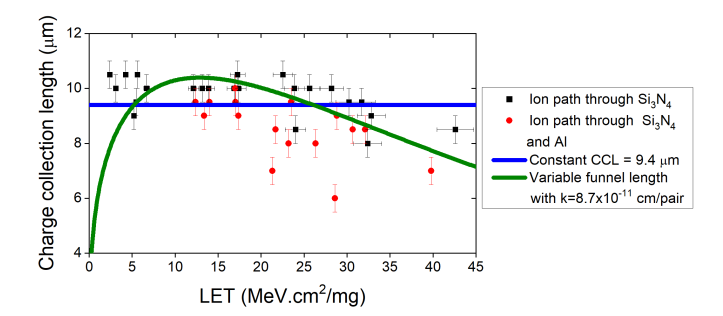


Fig. 12. Charge collection thickness that minimizes residues as a function of LET at the beginning of sensitive layer.

data points were obtained by simulating a silicon thickness in SRIM that absorbs the ion's energies given by the centroid and standard deviation of peaks relative to ions impinging on Si_3N_4 and $Si_3N_4 + Al$ (peaks H and L in Fig. 3). In the same figure, the plot of both funnel and constant CCL with the best-fit values found in this work shows that the variable funnel model better describes the experimental data, especially when considering the $Si_3N_4 + Al$ path, but the constant value approach cannot be completely discarded, given the uncertainties of both experimental data and simulations.

VI. CONCLUDING REMARKS

In this article, an experimental approach to describe the CCL and influence of metal/passivation layers for heavy-ion irradiation was presented, based on low-energy irradiations and statistical analysis. The behavior of reduced residual graphs shows that the variable funnel model, dependent on the incoming ion, is a better description of the CCL, as it is not tendentious for certain ion/energy conditions. It is shown that the previously reported shielding parameter k did not fit to observed data, and a new value was obtained with high precision, namely, $k = 8.7(2) \times 10^{-11}$ cm/pair for silicon devices. The analysis also provided the determination of the thickness of aluminum contacts and Si_3N_4 passivation layer as $1.28(2) \mu m$ and $0.72(6) \mu m$, respectively. The results obtained for Si_3N_4 thickness are compatible using both CCL models, showing the robustness of the data and analysis.

The low-energy heavy-ion irradiation and analysis methodology presented here has proven to be an effective tool for evaluating semiconductor devices without requiring prior knowledge of their internal structure or parameters, such as doping levels and charge carrier mobility. This approach can be applied to the study of emerging technologies, the characterization of COTS components, and for validating simulation models. The results obtained for the CCL significantly enhance the accuracy and reliability of single-event transient simulations in semiconductor devices.

REFERENCES

- S. Kirkpatrick, "Modeling diffusion and collection of charge from ionizing radiation in silicon devices," *IEEE Trans. Electron Devices*, vol. ED-26, no. 11, pp. 1742–1753, Nov. 1979.
- [2] C. Hsieh, P. C. Murley, and R. O'Brien, "A field-funneling effect on the collection of alpha-particle-generated carriers in silicon devices," *IEEE Electron Device Lett.*, vol. EDL-2, no. 4, pp. 103–105, Apr. 1981.

- [3] C. Hu, "Alpha-particle-induced field and enhanced collection of carriers," *IEEE Electron Device Lett.*, vol. ED-3, no. 2, pp. 31–34, Feb. 1982.
- [4] C.-M. Hsieh, P. C. Murley, and R. R. O'Brien, "Collection of charge from alpha-particle tracks in silicon devices," *IEEE Trans. Electron Devices*, vol. ED-30, no. 6, pp. 686–693, Jun. 1983.
- [5] C. Rossi, A. Chatel, and J.-M. Sallese, "Modeling funneling effect with generalized devices for SPICE simulation of soft errors," *IEEE Trans. Electron Devices*, vol. 68, no. 6, pp. 2633–2640, Jun. 2021.
- [6] F. B. McLean and T. R. Oldham, "Charge funneling in N- and P-type Si substrates," *IEEE Trans. Nucl. Sci.*, vol. NS-29, no. 6, pp. 2017–2023, Jun. 1982.
- [7] T. R. Oldham, F. B. McLean, and J. M. Hartman, "Revised funnel calculations for heavy particles with high dE/dx," *IEEE Trans. Nucl. Sci.*, vol. NS-33, no. 6, pp. 1646–1650, Jun. 1986.
- [8] M. Takada, T. Nunomiya, T. Ishikura, and T. Nakamura, "Charge-collection length induced by proton and alpha particle injected into silicon detectors due to funneling effect," *IEEE Trans. Nucl. Sci.*, vol. 56, no. 1, pp. 337–345, Feb. 2009.
- [9] S. Boorboor, S. A. H. Feghhi, and H. Jafari, "Funneling effect of alpha particles on the charge collection efficiency in N type silicon surface barrier detector," *Nucl. Instrum. Methods Phys. Res. B*, vol. 325, pp. 1–4, Apr. 2014.
- [10] Y. M. Aneesh, S. R. Sriram, K. R. Pasupathy, and B. Bindu, "An analytical model of single-event transients in double-gate MOSFET for circuit simulation," *IEEE Trans. Electron Devices*, vol. 66, no. 9, pp. 3710–3717, Sep. 2019.
- [11] C. Xu, Y. Liu, X. Liao, J. Cheng, and Y. Yang, "Machine learning regression-based single-event transient modeling method for circuitlevel simulation," *IEEE Trans. Electron Devices*, vol. 68, no. 11, pp. 5758–5764, Nov. 2021.
- [12] L. D. Edmonds, "A theoretical analysis of steady-state charge collection in simple diodes under high-injection conditions," *IEEE Trans. Nucl. Sci.*, vol. 57, no. 2, pp. 818–830, Apr. 2010.
- [13] L. D. Edmonds, "A theoretical analysis of the role of ambipolar diffusion in charge-carrier transport in a quasi-neutral region under high injection," *IEEE Trans. Nucl. Sci.*, vol. 58, no. 5, pp. 2459–2469, Oct. 2011.
- [14] L. D. Edmonds, "A proposed transient version of the ADC charge-collection model tested against TCAD," *IEEE Trans. Nucl. Sci.*, vol. 58, no. 1, pp. 296–304, Feb. 2011.
- [15] N. C. Hooten et al., "The significance of high-level carrier generation conditions for charge collection in irradiated devices," *IEEE Trans. Nucl. Sci.*, vol. 59, no. 6, pp. 2710–2721, Dec. 2012.
- [16] K. A. Moen and J. D. Cressler, "Measurement and modeling of carrier transport parameters applicable to SiGe BiCMOS technology operating in extreme environments," *IEEE Trans. Electron Devices*, vol. 57, no. 3, pp. 551–561, Mar. 2010.
- [17] C.-H. Yu, Y. Wang, M.-T. Bao, X.-J. Li, J.-Q. Yang, and F. Cao, "Impact of heavy-ion irradiation in an 80-V radiation-hardened splitgate trench power UMOSFET," *IEEE Trans. Electron Devices*, vol. 69, no. 2, pp. 664–668, Feb. 2022.
- [18] Y. Seo, M. Kang, J. Jeon, and H. Shin, "Prediction of alpha particle effect on 5-nm vertical field-effect transistors," *IEEE Trans. Electron Devices*, vol. 66, no. 1, pp. 806–809, Jan. 2019.
- [19] J. Liu, S. Yan, J. Xue, and Y. Wang, "Comparison of ionization track structure models for electronic devices of different sizes," *Nucl. Instrum. Methods Phys. Res. B*, vol. 444, pp. 43–49, Apr. 2019.
- [20] O. Musseau, "Charge collection and SEU mechanisms," *Radiat. Phys. Chem.*, vol. 43, nos. 1–2, pp. 151–163, Jan. 1994.
- [21] 3N163 3N164 P-Channel Enhancement Mode MOSFET, Linear Systems, Fremont, CA, USA, 2022.
- [22] M. S. Martínez-García et al., "Accuracy improvement of MOSFET dosimeters in case of variation in thermal parameters," *IEEE Trans. Nucl. Sci.*, vol. 62, no. 2, pp. 487–493, Apr. 2015.
- [23] P. R. P. Allegro et al., "Unsupervised machine learning application to identify single-event transients (SETs) from noise events in MOSFET transistor ionizing radiation effects," *Microelectron. Rel.*, vol. 142, Mar. 2023, Art. no. 114916.
- [24] V. A. P. Aguiar et al., "SAFIIRA: A heavy-ion multi-purpose irradiation facility in Brazil," *Rev. Sci. Instrum.*, vol. 91, no. 5, May 2020, Art. no. 053301.
- [25] C. Leroy and P.-G. Rancoita, Principles of Radiation Interaction in Matter and Detection. Singapore: World Scientific, 2009.
- [26] J. P. Biersack, M. D. Ziegler, and J. F. Ziegler, SRIM: The Stopping and Range of Ions in Matter. Chester, MD, USA: SRIM, 2008.